RSC Advances

PAPER

View Article Online
View Journal | View Issue

Cite this: *RSC Adv.*, 2026, **16**, 21591

Rapid discrimination of graphene oxide in a silk fiber/GO composite by temperature-dependent two-dimensional correlation FT-IR spectroscopy

Kum-Hui Kim,[a] Kyong-Sik Ju, *[a] Song-Hui Kim,[a] Hyon-Hui Ri,[a] Su-Bom Ri[a] and Kwang-Phil Kim[b]

In this study, a silk fiber/graphene oxide (GO) composite was directly obtained by feeding silkworm larvae with GO. Methods such as temperature-dependent Fourier transform infrared (FT-IR) spectroscopy, second-derivative analysis and two-dimensional (2D) correlation FT-IR spectroscopy were used to investigate the bonding interactions between GO and silk fibers in the silk fiber/GO composite. In addition, the silk fiber/GO composite was physically characterized by scanning electron microscopy (SEM) and thermogravimetric analysis (TGA). Temperature-dependent second-derivative FT-IR spectra of the reinforced silk fiber/GO composite showed a characteristic absorption band of GO at 1053 cm^{-1} and 40 °C, confirming the incorporation of GO into the silk fiber matrix. 2D correlation analysis of the temperature-dependent FT-IR spectra indicated that the asynchronous correlation intensity of the silk fiber/GO composite decreased 1.7-fold compared with that of the silk fiber, and the number of correlation peaks was significantly reduced, which suggests that GO present in the silk fiber/GO composite is thermally reduced with increasing temperature, resulting in enhanced thermally stability. The results of TGA showed that the silk fiber/GO composite exhibits higher decomposition temperatures than the silk fiber, which is in good agreement with the temperature-dependent 2D correlation analysis.

Received 4th February 2026
Accepted 6th April 2026

DOI: 10.1039/d6ra00969g

rsc.li/rsc-advances

1. Introduction

Graphene has become an ideal material for application in sensors, transistors and electrodes due to its excellent electrical, optical, thermal and mechanical properties.[1–9] Recently, research has been intensified on the development of various functional materials by the addition of graphene.[10,11] Graphene and its derivatives are widely used as fillers to enhance polymer composites due to their properties.[12–14] Silk fiber is a biopolymer with interesting properties such as excellent biocompatibility, biodegradability and high mechanical durability and is highly beneficial to environmental protection, which is already studied by many researchers in the past time.[15,16] Wang[17] reported that the mechanical properties of silk fibers obtained by the direct feeding of silkworm larvae with graphene or carbon nanotubes were improved due to changes in their secondary structure, confirming the presence of graphene and carbon nanotubes in silk fibers and silkworm feces by Raman spectroscopy. Wang *et al.*[21] fabricated functional silk fabrics with antibacterial activity and ultraviolet radiation protection by grafting GO nanosheet dispersions onto the silk fabric surface, indicating that there is one hydrogen bond between the silk fabric and GO by SEM analysis and FTIR and Raman spectroscopy. Bhattacharjee *et al.*[22] fabricated RGO and Ag/Cu nanoparticle (NP)-coated electroconductive silk fabrics, and their results indicated that modified silk fabrics exhibited outstanding hydrophobicity, enhanced thermal stability, and improved electrothermal and ultraviolet radiation protection, as characterized using ATR-FTIR, Raman, and UV spectroscopy and TGA.

Several methods such as temperature-dependent FT-IR spectroscopy, first- and second-derivative analysis and 2D correlation spectroscopy have been used to study graphene-based polymers. The conformational changes of polyvinyl alcohol (PVA) have been studied by temperature-dependent FT-IR spectroscopy at different temperatures.[18] Mahendia[19] studied the increase in glass transition temperature of reduced GO–PVA composites using the first derivative curves of temperature-dependent FT-IR spectra of reduced GO–PVA composites at different concentrations of reduced GO incorporated into PVA. In general, first and second-derivative techniques are both commonly used as spectral processing methods to resolve overlapping peaks.[20]

2D correlation FT-IR spectroscopy can successfully separate overlapping peaks and has been widely used to investigate the bonding mechanism in graphene-based composites, polymers

[a]*High-Tech Research and Development Center, Kim Il Sung University, Pyongyang, Democratic People's Republic of Korea. E-mail: ks.ju1025@ryongnamsan.edu.kp*
[b]*Faculty of Life Science, Kim Il Sung University, Pyongyang, Democratic People's Republic of Korea*

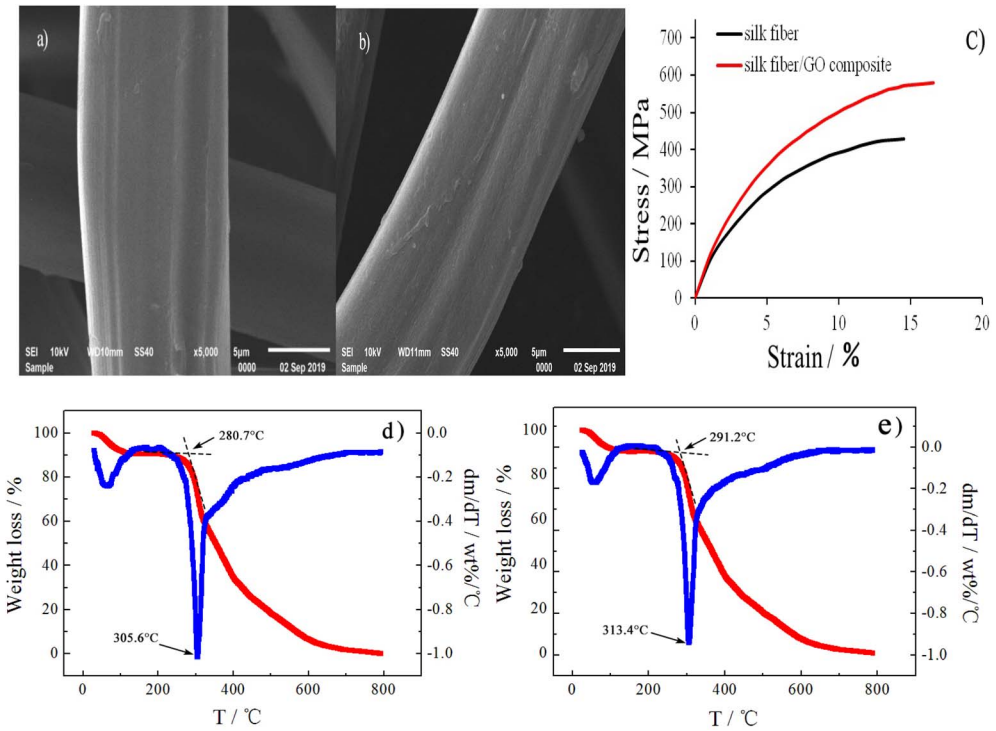

Fig. 1 SEM images of the silk fiber (a) and silk fiber/GO composite (b). (c) Stress–strain curves of silk fibers. TG and DTG curves of silk fiber (d), TG and DTG curves silk fiber/GO composite (e).

and carbon nanomaterials.[24–29] Su *et al.*[24] applied temperature-dependent FT-IR spectroscopy with generalized 2D correlation spectroscopy to investigate the phase transition mechanism of poly(*N*-isopropylacrylamide-*co*-2-hydroxyethyl methacrylate) (PNIPAM-*co*-HEMA) hydrogels. They suggested that the phase transition can be divided into two stages (21.8–31.4 °C and 31.4–36.5 °C), and the two phase-transition processes can be further divided into nine steps based on generalized 2D correlation analysis. Shao *et al.*[25] used second-derivative analysis and 2D FT-IR correlation spectroscopy to investigate conformation changes in glucose oxidase induced by adsorption onto GO sheets. The thermal reduction process of GO to graphene was already shown to occur in two stages by temperature-dependent 2D correlation and moving-window correlation, and the reduction mechanism was discussed in detail.[30]

In the study, a second-derivative method was combined with temperature-dependent FT-IR spectroscopy to detect the characteristic absorption bands of the epoxide and ether groups of GO in the silk fiber/GO composite. In addition, 2D correlation analysis was performed to investigate the bonding interactions between GO and silk fiber in the silk fiber/GO composite.

2. Experimental section

2.1 Material preparation

Graphene oxide was purchased from XFNANO, INC (Nanjing) and prepared using a modified Hummers' method.[31] GO was dispersed in deionized water at a concentration of 0.2 wt% under ultrasonication conditions for about 3 h. The suspension was uniformly sprayed on fresh mulberry leaves, which were then used as diets for the silkworms.

Bombyx mori silkworm larvae in the fifth instars were divided into two groups and raised at 25 °C and 20% relative humidity, being fed either with GO-treated leaves or normal mulberry leaves.

The cocoons obtained from the two groups were cut into appropriate sizes and washed with distilled water. They were then boiled in a 1-g per L Na_2CO_3 solution at 85 °C for 30 min to remove sericin, followed by washing with distilled water to remove residual Na_2CO_3. The degummed silk fibers were dried in an oven at 60 °C for 8 h.

The silk fibers obtained from silkworms fed with normal mulberry leaves and those fed with GO-treated leaves were denoted as the silk fiber and silk fiber/GO composite, respectively.

Table 1 Average diameters and mechanical properties of the two groups. Values are presented as mean ± SD

Types	Diameter (μm)	Tensile strength (MPa)	Elongation at break (%)	Young's modulus (GPa)
Silk fiber	12.2 ± 1.7	430 ± 25	14.7 ± 1.3	29.4 ± 1.2
Silk fiber/GO composite	11.3 ± 1.5	580 ± 32	16.4 ± 1.6	35.9 ± 1.4

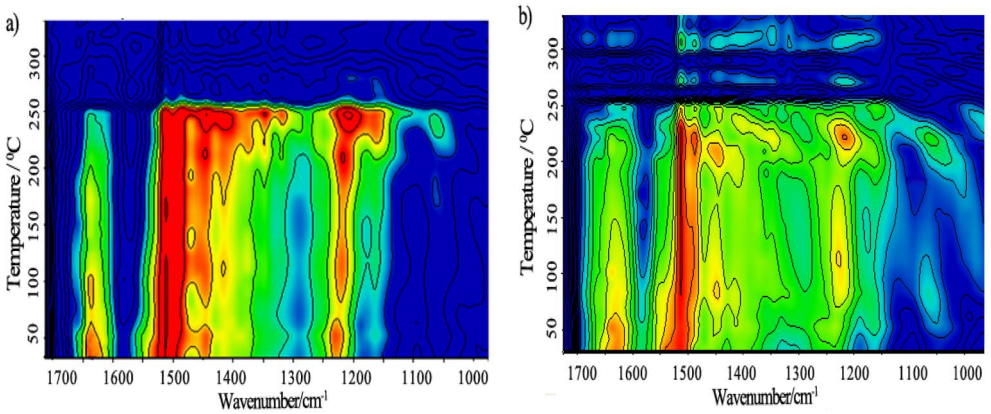

Fig. 2 Temperature-dependent FT-IR spectral profiles of the silk fiber (a) and silk fiber/GO composite (b).

2.2 Material characterization

2.2.1 Temperature-dependent 2D correlation FT-IR spectroscopy and Raman spectroscopy. Temperature-dependent FT-IR spectra were recorded using a Thermo Fischer Scientific (Madison, WI) Nicolet 6700 FT-IR spectrometer equipped with a heating cuvette and a temperature controller. The silk fibers were ground evenly in a mortar, formed into a thin film on a salt window, mounted in the heating cuvette, and then measured from 30 °C to 330 °C at a heating rate of 5 °C min^{-1}. Temperature-dependent FT-IR spectra were recorded in the 4000–400 cm^{-1} region with a resolution of 4 cm^{-1} and 32 scans. For reproducibility, measurements were performed in triplicate.

The synchronous and asynchronous 2D correlation FTIR spectra were calculated and processed using the MATLAB functions.[23]

Raman spectra were recorded on a LabRam HR800 Raman analyzer using a 532.17 nm Nd-YAG laser. For Raman measurements, 100 mg of degummed silk fiber/GO composite was dissolved in 20 mL of concentrated nitric acid, and this solution was diluted 30 times using distilled water. Finally, the dissolved silk fibroin was removed by vacuum filtration, and the resulting precipitate was used for Raman spectroscopic analysis.

2.2.2 TGA. A thermogravimetric analyzer (SHIMADZU TGA-50) was used to evaluate the thermal stability at a heating rate of 10 °C min^{-1} from room temperature up to 800 °C under N_2 at a flow rate of 20 mL min^{-1}. The TGA equipment was calibrated, and the experiments were performed at least twice to ensure repeatability.

2.2.3 Mechanical properties. For diameter measurement and mechanical testing, the first 20 m of the single fibers were collected and cut into 1 cm segments. First, the samples were placed on double-sided carbon adhesive tape. Then, the conducting process was performed for 80 s under the condition of 2.5 Pa, 40 mA, and 1.5 V using a JEC-3000FC AUTO FINE COATER (JEOL, Japan). Finally, the diameters were measured using the JSM-6610A SEM (JEOL, Japan). Average diameters of the silk fibers were measured at 20 different positions by SEM.

Mechanical testing was performed using an AG-X Plus instrument (Shimadzu, Japan) at a stretching speed of 1 mm min^{-1}, and the stress–strain curves were collected automatically by a computer.

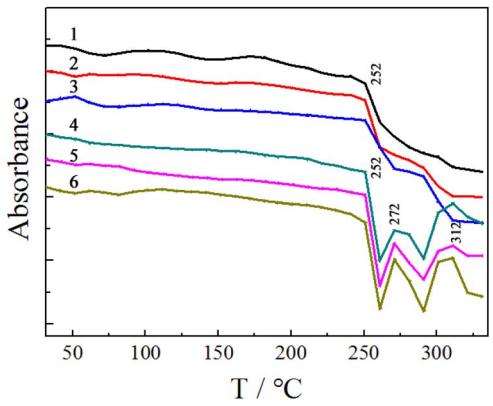

Fig. 3 Temperature-dependent FT-IR spectral intensity variation. Curves 1, 2, and 3 correspond to the amide I (1635 cm^{-1}), II (1519 cm^{-1}) and III (1230 cm^{-1}) bands of the silk fiber, respectively. Curves 4, 5, and 6 correspond to amide I, II and III bands of the silk fiber/GO composite, respectively.

3. Results and discussion

3.1 Properties of silk fiber

Fig. 1a and b show the SEM images of the silk fiber and silk fiber/GO composite, with average diameters of 12.2 μm and 11.3 μm, respectively. The SEM images show that the trace amount of GO incorporated into the silk fibers does not significantly affect the morphology of the silk fiber/GO composites.

Table 2 Maximum temperature change of spectral intensities corresponding to the amide bands in silk fiber and silk fiber/GO composite

	Silk fiber	Silk fiber/GO composite		
Wavenumber (cm^{-1})	T_1 (°C)	T_1 (°C)	T_2 (°C)	T_3 (°C)
1635 (amide I)	252	252	272	312
1520 (amide II)	252	252	272	312
1230 (amide III)	252	252	272	312

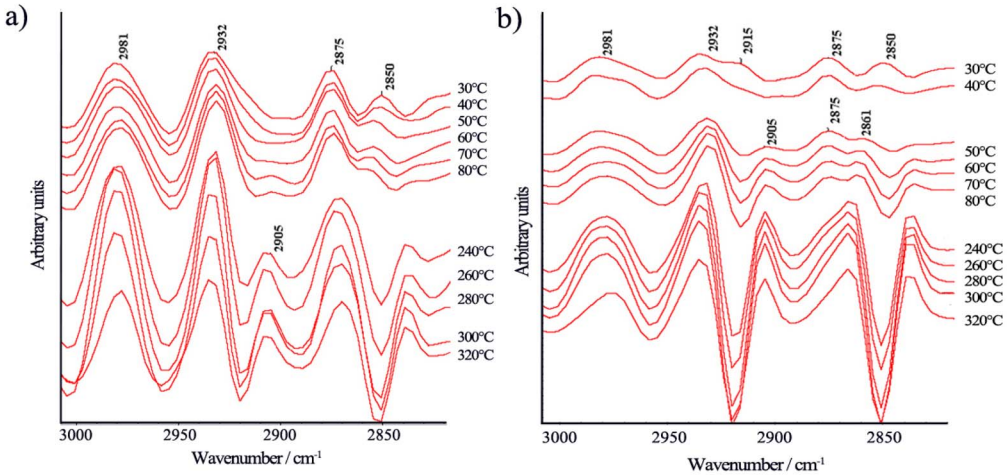

Fig. 4 Temperature-dependent second-derivative FT-IR spectra of the (a) silk fiber and (b) silk fiber/GO composite in the 3000–2800 cm^{-1} region.

The mechanical testing was performed on two groups. The typical stress–strain curves for the two groups are shown in Fig. 1c, which indicate higher values for the silk fiber/GO composite compared to the silk fiber. Table 1 shows a summary of the average diameters and mechanical properties of the two groups.

The tensile strength and Young's modulus of the silk fiber were 430 MPa and 29.4 GPa, respectively, while those of the silk fiber/GO composite were 580 MPa and 35.9 GPa.

TG and DTG (derivative thermogravimetric) curves of both fibers were recorded from room temperature up to 800 °C under an N_2 atmosphere to evaluate their thermal degradation properties, and the measurement results are shown in Fig. 1d and e. The initial weight loss observed around 100 °C for the two groups was due to water evaporation. The silk fiber exhibited significant weight loss at about 280.7 °C and showed a peak degradation temperature at about 305.6 °C. For the silk fiber/GO composite, these weight losses occurred at 291.2 °C and 313.4 °C, respectively, which can be attributed to the presence of GO in the silk fiber/GO composite.

The TG and DTG results demonstrate that the incorporation of GO improves the thermal stability of silk fibers, resulting in a slow thermal degradation process in the silk fiber/GO composite.

3.2 Interpretation of temperature-dependent FT-IR spectra of the silk fiber and silk fiber/GO composite

In order to further investigate the bonding mechanism in the silk fiber/GO composite with improved mechanical properties, the temperature-dependent changes in FT-IR spectral intensity of both fibers were compared. Fig. 2 shows the spectral intensity changes of both fibers with temperature in the 1700–1000 cm^{-1}

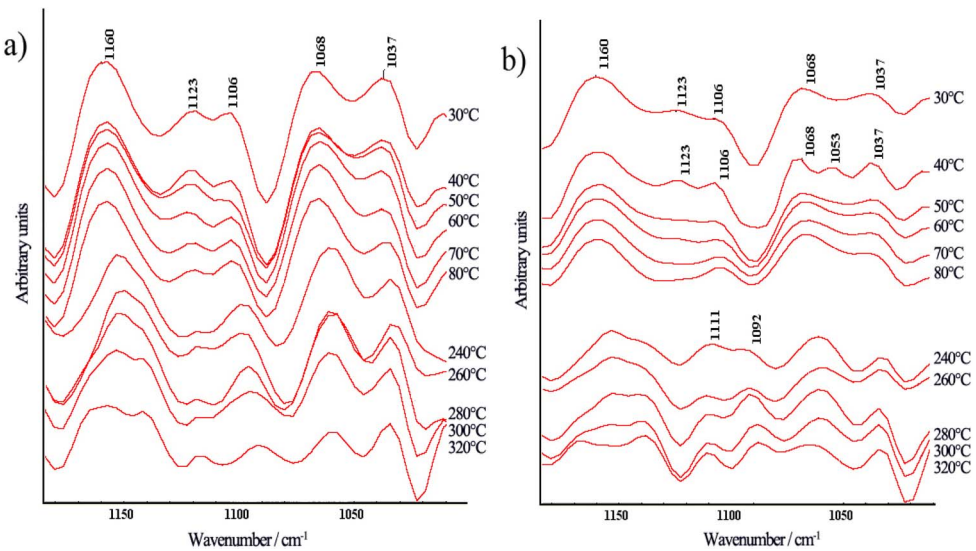

Fig. 5 Temperature-dependent second-derivative FT-IR spectra of the (a) silk fiber and (b) silk fiber/GO composite in the 1200–1000 cm^{-1} region.

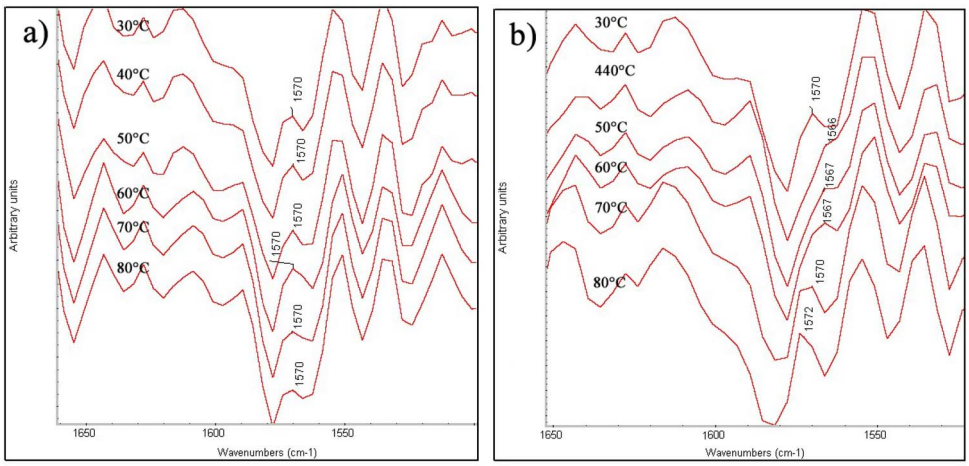

Fig. 6 Temperature-dependent second-derivative FT-IR spectra of the (a) silk fiber and (b) silk fiber/GO composite in the 1650–1500 cm^{-1} region.

region. As shown in Fig. 2a, the spectral intensity of the silk fiber remained unchanged above 250 °C, but as shown in Fig. 2b, the spectral intensities of the silk fiber/GO composite were changed continuously above 250 °C. This suggests that the silk fiber/GO composite has higher thermal stability compared to the silk fiber, and the observed difference in spectral intensity changes in both fibers may be attributed to structural changes in the silk fiber/GO composite.

Fig. 3 shows the temperature-dependent spectral intensity changes of the amide I (1635 cm^{-1}), amide II (1519 cm^{-1}) and amide III (1230 cm^{-1}) bands over the temperature range of 20 °C to 330 °C. The intensity changes of the amide I, II and III bands in both fibers were significantly different with increasing temperature. The spectra of silk fiber showed an absorbance change peaks at 252 °C, whereas the silk fiber/GO composite displayed three absorbance change peaks at 252 °C, 272 °C and 312 °C.

The maximum temperature changes of the spectral intensities corresponding to the amide bands in the silk fiber and silk fiber/GO composite are shown in Table 2. The temperature-dependent FT-IR spectra show that the thermal behavior of the silk fibers/GO composite differs significantly from that of the silk fiber. These differences between the two fibers were investigated using second-derivative treatment of the temperature-dependent FT-IR spectra. Overlapping peaks can be resolved into two or more peaks by applying the second-derivative treatment. The second-derivative spectra were obtained using a Savitzky–Golay filter through 7-point smoothing.

The second-derivative spectra are more complex and significantly narrower than the first-derivative spectra, which is preferred for analyzing the thermal behavior of silk fibers/GO composite. The temperature-dependent second-derivative FT-IR spectra of the two fibers, recorded upon heating from 30 °C to 320 °C in the 3000–2800 and 1200–1000 cm^{-1} regions, are illustrated in Fig. 4 and 5.

The temperature-dependent second-derivative FT-IR spectra of both fibers in the 3000–2800 cm^{-1} region were evidently different. The bands at 2932, 2915 and 2850 cm^{-1} can be assigned to the stretching vibrations of the methylene group of glycine, and the bands at 2981, 2861 and 2905 cm^{-1} can be attributed to the stretching vibrations of the methyl group of alanine and the tertiary CH stretching vibrations of alanine. The second-derivative FT-IR spectra of the silk fiber (Fig. 4a) showed no changes between 30 °C and 70 °C. In contrast, in the silk fiber/GO composite (Fig. 4b), a new peak at 2905 cm^{-1} appeared at 50 °C, and the band intensity increased.

The most obvious differences between the temperature-dependent second-derivative FT-IR spectra in Fig. 5a and b were observed at 40 °C and 50 °C. A peak at 1053 cm^{-1} appeared at 40 °C in the silk fiber/GO composite, representing the characteristic absorption band of the C–O–C groups in GO.[30] In addition, the peaks at 1053 cm^{-1} and 1123 cm^{-1} disappeared simultaneously at 50 °C. This can be attributed to the

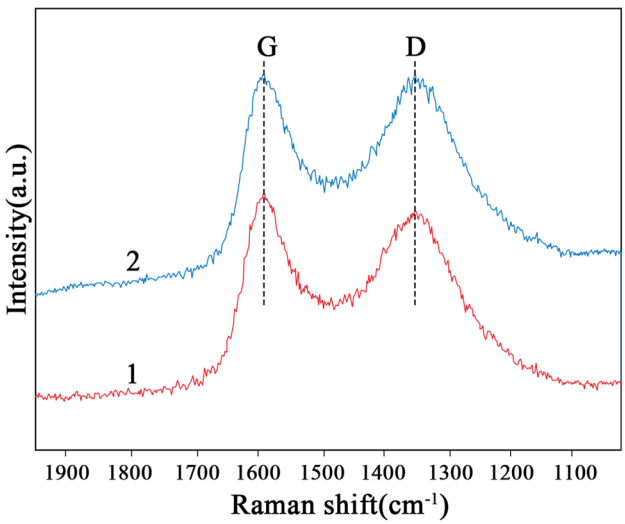

Fig. 7 Raman spectra of the (1) GO and (2) precipitate obtained from the silk fiber/GO composite in the 2000–1000 cm^{-1} region.

weakening or breaking of intermolecular bonds between GO and the silk fiber with increasing temperature.

Fig. 6 shows the temperature-dependent second-derivative infrared spectra of both fibers in the 1650–1500 cm^{-1} region recorded upon heating from 30 °C to 80 °C. The C=C skeletal vibrations in GO appear near 1570 cm^{-1}. As shown in Fig. 6a, the absorbance intensity at 1570 cm^{-1} for the silk fiber hardly changes with increasing temperature. On the other hand, for the silk fiber/GO composite (Fig. 6b), the absorbance intensity at 1570 cm^{-1} decreases at 30 °C and 40 °C, accompanied by a wavenumber shift to 1566 cm^{-1}. The absorbance intensity increases and shifts towards higher wavenumbers above 50 °C. Hence, it indicates an increase in the band intensity corresponding to the C=C skeletal vibrations at 1570 cm^{-1}, relative to the decrease in the C–O bands at 1053 cm^{-1}, suggesting that the trace amount of GO incorporated into the silk fibers is thermally reduced upon heating.

The above results can confirm the incorporation of GO into the silk fiber/GO composite, but they provide limited information about the bonding interactions between the silk fiber and GO.

Fig. 7 shows the Raman spectra of GO and the precipitate obtained from the silk fiber/GO composite. As shown in Fig. 7(1), the Raman spectrum of GO exhibits a G band at 1584 cm^{-1} and a D band at 1346 cm^{-1}. The G band at 1584 cm^{-1} is related to the sp^2 graphite structure, and the D band at 1346 cm^{-1} is assigned to the local defects in the carbon material,[17] which is also evident in the Raman spectrum of the precipitate obtained from the silk fiber/GO composite (Fig. 7(2)). The results indicate that GO was incorporated into the silk fibers through the diet. However, using Raman spectroscopy to confirm the presence of GO in silk fiber composites has the disadvantage of very complex sample pretreatment.

2D correlation spectroscopy has been used as a powerful tool to analyze changes in physical and chemical processes in response to external perturbations such as temperature.[32] 2D

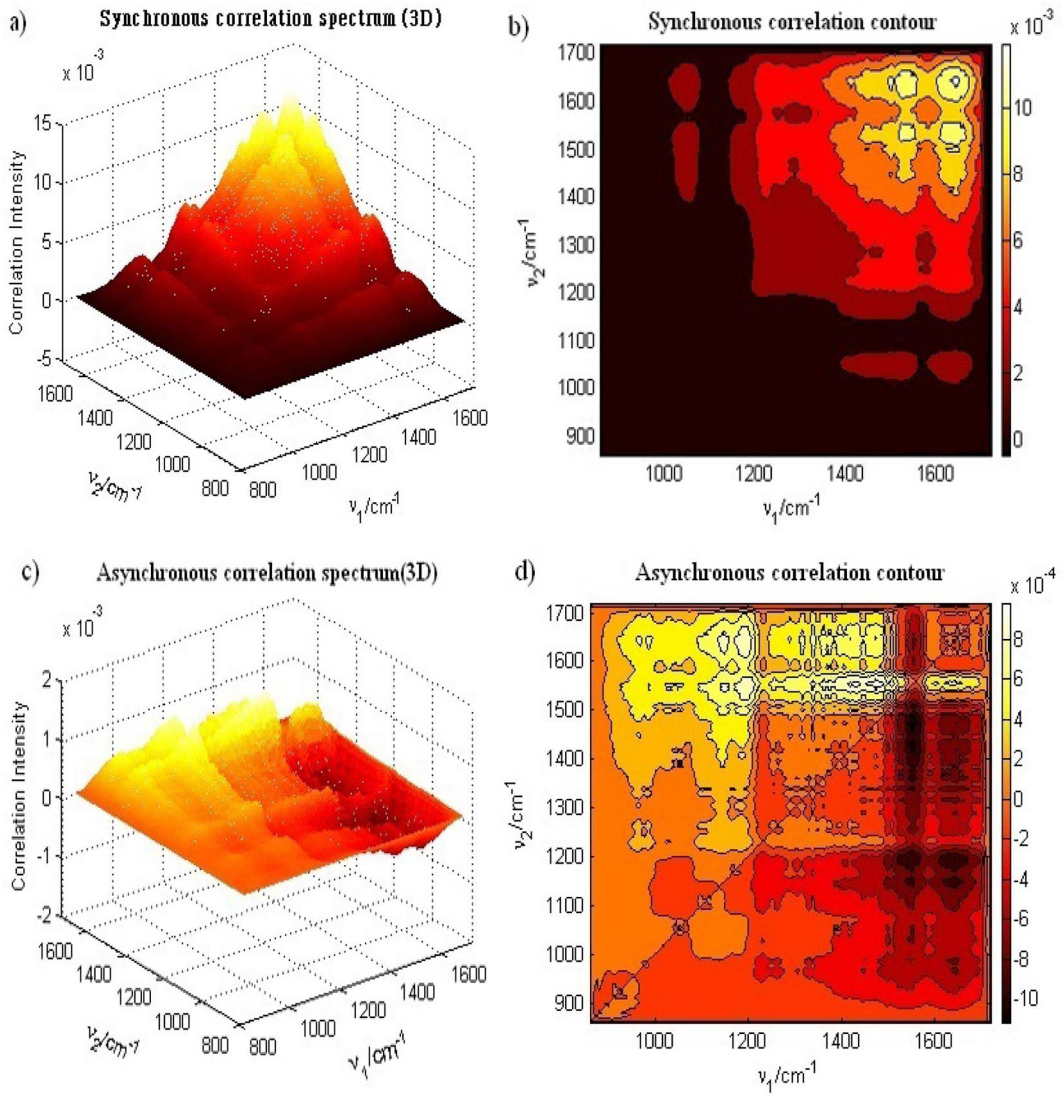

Fig. 8 Temperature-dependent 2D correlation FT-IR spectra of the silk fiber in the 1700–800 cm^{-1} region: synchronous (a) and asynchronous (c) correlation spectra, and synchronous (b) and asynchronous (d) correlation contour maps.

Table 3 Correlation wavenumbers, signs of correlation peaks and directions of intensity changes in the synchronous and asynchronous temperature-dependent 2D correlation spectra of the silk fiber

	Correlation wavenumbers (cm^{-1})		Sign of correlation peaks	Direction of intensity changes in the dynamic spectra	
	N_x	ν_y		ν_x	ν_y
Asynchronous correlation spectra	1643	1643	0	↓	
	1540	1540	0	↓	
	1041	1041	0	↓	
Asynchronous correlation spectra	1643	1540	—	↓	↘↗↘
	1508	1415	—	↓	↘↗↘
	1508	1288	—	↓	↘↗↘
	1508	1187	—	↓	↘↗↘
	1643	1187	+	↓	↓
	1643	1187	+	↓	↓

Table 4 Assignments of the correlation wavenumbers listed in Table 3[33]

Frequency (cm^{-1})	Assignments
1041	C–N stretching vibration of phenylalanine
1187	C–N stretching vibration of tyrosine
1288	Amide II in β-sheet conformation
1415	CH_2 bending in asparagine
1508	Amide II [N–H bending and C–N bending]
1540	Amide II [peptide bond 60% N–H bending and 40% C–N bending]
1643	Amide I in β-sheet conformation

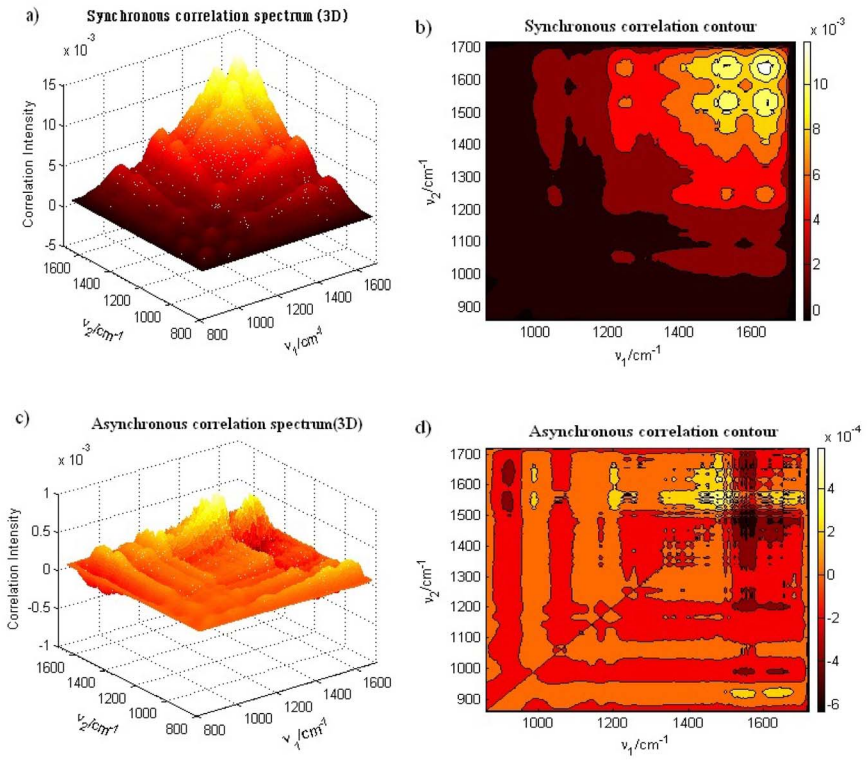

Fig. 9 Temperature-dependent 2D correlation FT-IR spectra of the silk fiber/GO composite in the 1700–800 cm^{-1} region: synchronous (a) and asynchronous (c) correlation spectra, and synchronous (b) and asynchronous (d) correlation contour maps.

Table 5 Correlation wavenumbers and their directions of intensity changes in the synchronous and asynchronous temperature-dependent 2D correlation of the silk fiber/GO composite

	Correlation wavenumbers		Sign of correlation peaks	Direction of intensity changes in the dynamic spectra	
	ν_x (cm^{-1})	ν_y (cm^{-1})	ν_x (cm^{-1})	ν_x (cm^{-1})	ν_y (cm^{-1})
Synchronous correlation spectra	1647	1647	+	↓	
	1540	1540	+	↓	
	1261	1261	+	↘↗↘	
Asynchronous correlation spectra	1542 and 1643	921	+	↓	↘↗↘
	1542 and 1643	990	—	↓	↘↗↘
	1542 and 1643	1203	—	↓	↘↗↘
	1666	1566 and 1554	+	↓	↓

correlation analysis of temperature-dependent FT-IR spectra was carried out to compare the temperature behavior and bonding modes of the silk fiber and silk fiber/GO composite.

3.3. 2D correlation FT-IR analysis of the silk fiber and silk fiber/GO composite

3.3.1 2D correlation FT-IR analysis of the silk fiber. Fig. 8 shows the generalized 2D correlation spectra of the temperature-dependent FT-IR spectra of the silk fiber.

In Fig. 8a, the auto-correlation spectrum shows prominent auto-correlation peaks at 1643, 1540 and 1041 cm^{-1}; on the other hand, the asynchronous correlation spectrum (Fig. 8b) shows the cross-correlation peaks between them. The asynchronous correlation spectrum (Fig. 8d) shows the cross-correlation peaks between 1643, 1540, 1508 and 1643 cm^{-1}.

The correlation wavenumbers in the 2D correlation spectra, along with the signs of the synchronous and asynchronous correlation peaks and the direction of intensity changes at each corresponding wavenumber in the dynamic spectra, are summarized in Table 3.

The assignments of the correlation wavenumbers listed in Table 3 are summarized in Table 4.

Based on the results in Tables 3 and 4, the directions of intensity changes and the order of spectral variations at individual wavenumbers can be derived as follows: the spectral intensities at 1643 and 1508 cm^{-1} decrease prior to the spectral intensity change (↘↗↘) observed at 1540, 1415, 1288, and 1187 cm^{-1}. Subsequently, a further decrease in spectral intensity at 1187 cm^{-1} occurs with increasing temperature.

3.3.2 2D correlation FT-IR analysis of silk fiber/GO composite. Fig. 9 shows the generalized 2D correlation spectra of the temperature-dependent FT-IR spectra of silk fiber/GO composite.

The 2D correlation spectra of the silk fiber (Fig. 8) and the silk fiber/GO composite (Fig. 9) show significant differences in the synchronous and asynchronous correlation spectra. The intensity ranges of the synchronous and asynchronous correlation spectra for the silk fiber are -5.6×10^{-4}–0.0123 and −0.0011–0.0011, respectively, while for the silk fiber/GO composite, they are -5.14×10^{-4}–0.013 and -6.402×10^{-4}–6.402×10^{-4}, respectively. The intensities of the synchronous correlation spectra are similar between the two fibers, but the intensities of the asynchronous correlation spectra differ markedly. The asynchronous correlation strength of the silk fiber/GO composite decreases by about 1.7-fold compared to that of the silk fiber. The silk fiber/GO composite shows the smaller correlation intensities compared to the silk fiber upon heating; *i.e.*, it was thermally stable 1.7-fold. In addition, the synchronous correlation spectra of the silk fiber/GO composite show new peaks at 1261 cm^{-1} and 926 cm^{-1} compared to the silk fiber (Fig. 9b). The asynchronous correlation spectra of the silk fiber/GO composite also differed greatly, with a significant decrease in the number of asynchronous correlation peaks compared to that of the silk fiber (Fig. 9d). The decrease in the correlation intensity and the decrease in the number of these

Table 6 Assignments of the FT-IR absorption bands of GO[10,11,30,34]

Frequency (cm^{-1})	Assignments
1566	C=C stretching of the sp^2-hybridized carbon atoms[30,34]
1261	C–O stretching vibration of epoxide[34]
1203	C–O stretching of epoxide[10,11]

Table 7 Assignments of the correlation wavenumbers shown in Table 5

Frequency (cm^{-1})	Direction of intensity changes	Assignments
921	↘↗↘	–C(CH_3) skeletal vibration
990	↘↗↘	Gly–Ala C–C skeletal stretching in silk fiber
1203	↓	C–O stretching of epoxide in GO
1261	↓	C–O stretching vibration of epoxide
1523	↓	Amide II [N–H bending and C–N bending]
1542 and 1554	↓	Amide II [peptide bond 60% N–H bending and 40% C–N bending]
1566	↓	C=C stretching of the sp^2-hybridized carbon atoms
1643 and 1647	↓	Amide I in β-sheet conformation
1666	↓	Amide I in antiparallel β-sheet conformation

correlation peaks in the asynchronous correlation spectra of the silk fiber/GO composite indicate that the correlation intensity changes in FT-IR absorption bands upon external heating is small compared to that of the silk fiber.

Table 5 shows the correlation wavenumbers of the synchronous and asynchronous temperature-dependent correlation spectra for the silk fiber/GO composite and their intensity change directions.

The assignments of the interested FT-IR absorption bands of GO are summarized in Table 6.

Based on the signs and directions of the correlation signals in the 2D correlation spectra of the silk fiber/GO composite, the order of intensity changes of the absorption bands with increasing temperature can be derived as follows:

The spectral intensities at 1542, 1643 and 1666 cm^{-1} decrease, while those at 990 and 1203 cm^{-1} show a decrease → increase → decrease pattern. On the other hand, the spectral intensities at 990 and 1203 cm^{-1} decrease prior to the spectral intensity changes at 1542 and 1643 cm^{-1}. Subsequently, the spectral intensity at 921 cm^{-1} decreases, followed by a spectral intensity decreases at 1666, 1573, 1566 and 1554 cm^{-1} with increasing temperature.

In summary, the order of intensity changes is 990 and 1203 cm^{-1} (↘↗↘) → 1542, 1643, and 1666 cm^{-1} (↓) → 921 cm^{-1} (↘↗↘) → 1554 cm^{-1} (↓) → 1566 cm^{-1} (↓) → 1666 cm^{-1} (↓).

Table 7 lists the assignments of the correlation wavenumbers shown in Table 5.

The comparison of the 2D correlation analysis results for silk fiber and silk fiber/GO composites shows significant differences. In silk fibers, changes in the amide I and II bands, corresponding to the silk fiber structure, occur first, and then structural changes occur in order. In silk fiber/GO composites, spectral intensity changes occur first at the 990 cm^{-1} band, corresponding to the C–C stretching vibration of the glycine–alanine units in silk fiber, and at the 1203 cm^{-1} band, corresponding to the C–O stretching vibration of the epoxide group in GO, followed by sequential structural changes in the silk fiber. Therefore, it can be seen that the thermal stability of the silk fiber/GO composite is improved compared with that of silk fiber. In addition, as shown in Tables 3 and 4, the number of asynchronous correlation peaks in the silk fiber/GO composite decreased compared to silk fiber. From these results, it can be expected to be due to the rearrangement of the silk fiber structure by GO, resulting in a more stable structure.

These results demonstrate that the relationship between the structure and thermal stability of the silk fiber and the silk fibers/GO composite can be effectively investigated by temperature-dependent 2D correlation FT-IR spectroscopy.

4. Conclusions

Temperature-dependent infrared spectra of the silk fiber and the silk fiber/GO composite demonstrate that the spectral intensity changes of the amide I, II and III bands with increasing temperature are significantly different. The silk fiber exhibits an absorbance change at 252 °C, and the silk fiber/GO composite shows three absorbance change peaks at 252 °C, 272 °C and 312 °C. Temperature-dependent second derivative FT-IR spectra reveal the presence of a characteristic absorption band of GO at 40 °C.

The characteristic peaks of GO were observed in the 2D correlation FT-IR spectra of the silk fiber/GO composite, which confirmed the incorporation of GO into the silk fiber/GO composite. It was also found that the asynchronous correlation intensity of the silk fiber/GO composite decreased by around 1.7-fold compared to that of the silk fiber with increasing temperature, and the number of correlation peaks was significantly reduced, indicating enhanced thermal stability due to the presence of GO in the silk fiber/GO composite.

The results of TGA are in good agreement with the temperature-dependent 2D correlation FT-IR analysis. This study shows the usefulness of temperature-dependent 2D correlation FT-IR spectroscopy for detecting trace amounts of GO in GO composites and for investigating their bonding interactions with the matrix. The optimal content of GO required to produce silk fibers with the desired mechanical strength should be determined in future work.

Conflicts of interest

There are no conflicts to declare.

Data availability

The data that support the findings of this study are available from the corresponding authors upon reasonable request.

Acknowledgements

This work was supported by the State Commission of Science and Technology in the DPR of Korea.

References

1 S. Bai and X. Shen, *RSC Adv.*, 2012, **2**, 64.
2 Y. Zhu, S. Murali, W. Cai, X. Li, J. W. Suk, J. R. Potts and R. S. Ruoff, *Adv. Mater.*, 2010, **22**, 3906.
3 X. Huang, X. Qi, F. Boey and H. Zhang, *Chem. Soc. Rev.*, 2012, **41**, 666.
4 N. O. Weiss, H. Zhou, L. Liao, Y. Liu, S. Jiang, Y. Huang and X. Duan, *Adv. Mater.*, 2012, **24**, 5776.
5 R. J. Young, I. A. Kinloch, L. Gong and K. S. Novoselov, *Compos. Sci. Technol.*, 2012, **72**, 1459.
6 M. J. Allen, V. C. Tung and R. B. Kaner, *Chem. Rev.*, 2010, **110**, 132.
7 Y. Xu and G. Shi, *J. Mater. Chem.*, 2011, **21**, 3311.
8 Q. Zhang, *et al.*, *Mater. Sci. Eng., C*, 2017, **77**, 37.
9 E. F. D. Januário, *et al.*, *Sci. Total Environ.*, 2021, **789**, 147957.
10 A. W. Yang, *et al.*, *Appl. Surf. Sci.*, 2015, **346**, 443.
11 Q. X. Ren, *et al.*, *Mater. Sci. Eng., C*, 2016, **68**, 308.
12 Y. Y. Zhang, C. M. Wang, Y. Cheng and Y. Xiang, *Carbon*, 2011, **49**, 4511.
13 K. Hu, M. K. Gupta, D. D. Kulkarni and V. V. Tsukruk, *Adv. Mater.*, 2013, **25**, 2301.
14 N. Wei, X. Peng and Z. Xu, *ACS Appl. Mater. Interfaces*, 2014, **6**, 5877.
15 D. L. Wen, *et al.*, Microsyst, *Nanoeng*, 2021, **7**, 35.
16 S. N. L. Pilley, *et al.*, *Environ. Sci. Pollut. Res.*, 2022, **29**, 56606.
17 Q. Wang, C. Y. Wang, M. C. Zhang, M. Q. Jian and Y. Y. Zhang, *Nano Lett.*, 2016, **16**, 6695.
18 S. Han, *et al.*, *Spectrochim. Acta, Part A*, 2015, **139**, 37.
19 S. Mahendia, *et al.*, *J. Mol. Struct.*, 2016, **1111**, 46.
20 Y. S. Hong, *et al.*, *Sci. Total Environ.*, 2019, **651**, 1969.
21 S. D. Wang, K. Wang, Q. Ma and C. X. Qu, *Mater. Sci. Eng., C*, 2020, **107**, 8.
22 S. Bhattacharjee, C. R. Macintyre, *et al.*, *Adv. Mater. Interfaces*, 2020, **7**, 2000814.
23 I. Noda, *Appl. Spectrosc.*, 1993, **47**, 1329.
24 G. Su, T. Zhou, X. Liu and Y. Ma, *Polym. Chem.*, 2017, **8**, 865.
25 Q. Shao, Y. Qian, P. Wu, H. Zhang and C. Cai, *Colloids Surf., B*, 2013, **109**, 115.
26 I. Noda, *J. Mol. Struct.*, 2018, **1160**, 471.
27 Y. Liu, W. Li, L. Hou and P. Wu, *RSC Adv.*, 2014, **4**, 24263.
28 W. Guo, J. Chen, S. Sun and Q. Zhou, *J. Phys. Chem. C*, 2016, **120**, 7451.
29 I. Noda, *Appl. Spectrosc.*, 1993, **47**, 1329.
30 Y. Ren, T. Zhou, G. Su and Y. Ma, *Vib. Spectrosc.*, 2018, **96**, 32.
31 W. S. Hummers and R. E. Offeman, *J. Am. Chem. Soc.*, 1958, **80**, 1339.
32 S. H. Kim, K. S. Ju, *et al.*, *Chem. Phys. Lett.*, 2020, **742**, 137146.
33 M. A. Koperska, *et al.*, *Polym. Degrad. Stab.*, 2014, **105**, 185.
34 M. Acik, G. Lee, C. Mattevi, M. Chhowalla, K. Cho and Y. J. Chabal, *Nat. Mater.*, 2010, **9**, 840.